Nitrogen Fixation

DOI: 10.1002/anie.201303000

Analysis of the Magnetic Properties of Nitrogenase FeMo Cofactor by Single-Crystal EPR Spectroscopy**

Thomas Spatzal, Oliver Einsle, and Susana L. A. Andrade**

Dedicated to Professor Douglas C. Rees on the occasion of his 60th birthday

The enzyme nitrogenase reduces dinitrogen and a variety of other substrates at a unique [Mo:7Fe:9S:C]:(*R*)-homocitrate–iron–molybdenum cluster, the FeMo cofactor (FeMoco).[1] The cluster has been characterized in high structural detail,[2] but its functional properties and its precise role in biological nitrogen fixation remain enigmatic. Nitrogenase is the only enzyme known to catalyze the reductive fixation of atmospheric N_2 to bioavailable ammonium, NH_4^+, coupled to the production of H_2 and the hydrolysis of ATP. It is a two-component metalloenzyme that assembles under turnover conditions and consists of the MoFe protein ($NifD_2K_2$) and the Fe protein ($NifH_2$).[3] Fe protein is the site of ATP hydrolysis and serves as the electron donor for the MoFe protein. The $\alpha_2\beta_2$ heterotetrameric MoFe protein contains two copies of the FeMo cofactor and of the [8Fe:7S] P-cluster, an electron-transfer site. FeMo cofactor is coordinated to a homocitrate molecule and two protein ligands, α-C275 and α-H442, in the *Azotobacter vinelandii* enzyme (Figure 1 A). The cluster has pseudo-D_3 symmetry that is broken only by the apical molybdenum ion (Figure 1 B,C). The seven iron atoms show fourfold coordination with near-tetrahedral geometry. The light atom at the cofactor center was recently identified as carbon, but its function remains unclear.[4]

In spite of decades of extensive studies, the catalytic activity and the associated magnetic properties of FeMo cofactor are poorly understood. When isolated in the presence of dithionite, MoFe protein contains the active site cluster in a $S = 3/2$ ground state ($FeMoco^N$).[5] Chemical oxidation leads to a reversible transition at −42 mV, yielding a diamagnetic state ($FeMoco^{Ox}$), which was characterized by Mössbauer and MCD spectroscopy, but may not be of physiological relevance.[6] Using reduced Fe protein, $FeMoco^N$ can be further reduced to a $FeMoco^R$ state ($S \geq 1$), which could not be obtained through chemical or electrochemical reduction.[7] To date, the $S = 3/2$ $FeMoco^N$ is by far the best-characterized state, and it was investigated by EPR, Mössbauer, ENDOR, XANES, and EXAFS spectroscopy.[5b,6c,8] From this, two prevailing hypotheses for the electron distribution within the cluster have emerged.

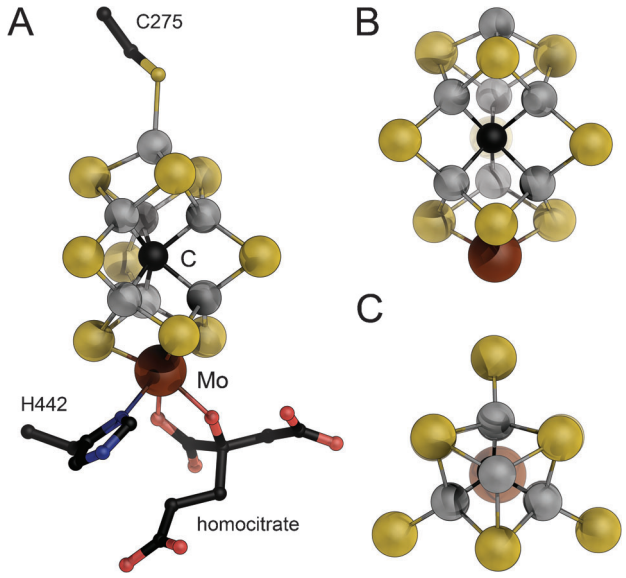

Figure 1. Structure of the FeMo cofactor [Mo:7Fe:9S:C]:(*R*)-homocitrate located in the α-subunit of the nitrogenase MoFe protein from *Azotobacter vinelandii*. A) The metal cluster is coordinated by two amino acids, α-C275 and α-H442. Fe gray, Mo brown, S yellow, C black, N blue, O red. B) View along the pseudo-twofold symmetry axis. C) View along the threefold axis of the FeMoco (from PDB ID 3U7Q).

The first model describes the oxidation states of the metal ions as $[Mo^{4+}:Fe^{3+}:6Fe^{2+}]$, while in the second model, supported by ENDOR and XANES data, the resulting assignment is $[Mo^{4+}:3Fe^{3+}:4Fe^{2+}]$.[8a,c,9] As both the exact electronic configuration and the redox-state assignments for the individual atoms remain controversial, an unambiguous theoretical derivation of the exact spin-coupling situation has not been achieved. DFT calculations in combination with broken-symmetry (BS) approaches were used to obtain information about the intrinsic spin coupling of the FeMo cofactor.[8c,9a,10] With an overall $S = 3/2$ resting spin state and a presumed $[Mo^{4+}:3Fe^{3+}:4Fe^{2+}]$ configuration, 10 different spin configurations are possible which all result in a 4(up)/

[*] Dr. T. Spatzal,[+] Prof. O. Einsle, Prof. S. L. A. Andrade
Institut für Biochemie, Albert-Ludwigs-Universität Freiburg
Albertstrasse 21, 79104 Freiburg (Germany)
and
BIOSS Centre for Biological Signalling Studies
Hebelstrasse 25, 79104 Freiburg (Germany)
E-mail: einsle@bio.chemie.uni-freiburg.de
andrade@bio.chemie.uni-freiburg.de
Homepage: http://portal.uni-freiburg.de/biochemie
[+] Present address: Howard Hughes Medical Institute (HHMI) and Division of Chemistry and Chemical Engineering
California Institute of Technology
1200 East California Boulevard, Pasadena CA 91125 (USA)

[**] This work was supported by Deutsche Forschungsgemeinschaft (grant AN 676/3 to S.L.A.A., grant EI 520/7 to O.E.) and the European Research Council.
Supporting information for this article is available on the WWW under http://dx.doi.org/10.1002/anie.201303000.

3(down) spin-coupling alignment, wherein the BS7 coupling scheme best describes the experimental data.[11] The interstitial carbon atom in the cluster was included neither in these calculations nor in earlier analyses of experimental data.[4]

EPR spectroscopy can be a powerful tool for gaining spatial information about the magnetic properties of a metal center that is directly linked to its electronic structure. Used on ordered single crystals, EPR spectroscopy can be used to determine the relative orientation of the principal axes of the magnetic **g** tensor of a paramagnetic center with respect to its structure.

Single crystals of *Clostridium pasteurianum* MoFe protein were previously studied with EPR by Hoffman and coworkers, but at the time no structural information was available.[12] Here we report the analysis of single-crystal EPR measurements on MoFe protein from *Azotobacter vinelandii*, which in combination with X-ray crystallography defines the orientation of the magnetic **g** tensor with respect to FeMoco geometry. Measurements were carried out at thfe X-band, using dithionite-reduced MoFe protein crystals with dimensions of approximately $1.0\times0.8\times0.8$ mm^3. The principal axes of the **g** tensor of the $S=3/2$ FeMoco^N state, derived from powder spectra, are $g_x=2.01$, $g_y=3.65$, and $g_z=4.31$, and are in agreement with a simulation based on a $M_s=\pm1/2$ Kramer's doublet transition at a rhombicity of $E/D=0.053$. This signal arises exclusively from FeMoco, as the P-cluster in its P^N state contains only Fe^{II} and thus is diamagnetic.

MoFe protein crystallized in the monoclinic space group $P2_1$ with one or two heterotetramers per asymmetric unit and two asymmetric units per unit cell. In the case of the larger unit cell, the noncrystallographic symmetry operation relating the two tetramers was almost a pure translation, so that always only up to four distinct and magnetically independent resonances could be observed (Figure 2). Due to fortuitous orientation of the crystal with one unit cell plane normal to the magnetic field vector $\mathbf{B}_1$, the number of resonance features was in some instances reduced to two, leading to a significant simplification of the evaluation process for some of the examined crystals. The crystals showed a distinct angular dependence of the EPR signals within the limits of the principal axes of the **g** tensor (Figure 2A, Figure 3A), and

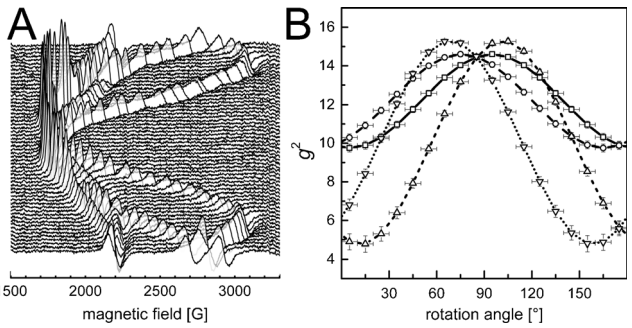

Figure 2. Single-crystal EPR measurements. A) X-band spectra of an *A. vinelandii* MoFe protein crystal, recorded in 3° steps over a range of 180°. Four EPR signals represent the magnetically distinct metal centers in the crystal unit cell. B) Sinusoidal fit of the $\mathbf{g}^2$ values for all signals. The symbols represent the four magnetically distinct FeMo cofactors in the unit cell.

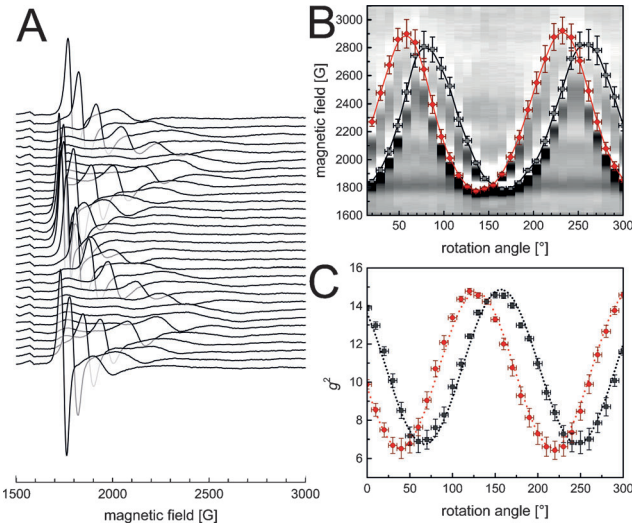

Figure 3. A) Symmetry-reduced single-crystal X-band spectra of MoFe protein, recorded over a range of 300°. Two resonances are resolved, corresponding to only two magnetically distinct centers when the rotation axis is parallel to the *b* axis of the crystal. B) Angular dependence of the EPR signals derived from the spectra, superimposed on a 2D contour plot. The *x*-axis errors are due to technical factors, in particular the positional freedom of the glass capillary in the EPR tube, while the *y*-axis errors, determined as peak width at half-height, are due to line-broadening. The superposition was the basis for the subsequent simulation. C) Sinusoidal fit of the $\mathbf{g}^2$ values, analogous to Figure 2B. The symbols represent the two magnetically distinct FeMo cofactors in the unit cell.

the expected sinusoidal shape for the $\mathbf{g}^2$ values with a periodicity of 180° (Figure 2B, Figure 3C).

Orientation-dependent line-broadening of the EPR signals, as a result of **g** strain (Figure 3A), was frequently observed at higher field.[12] In order to determine the signal positions from individual spectra more precisely, two-dimensional contour plots were generated (Figure 3B), and the first- and second-derivative plots were inspected at higher field. Signal positions were determined from peak positions of integrated spectra. The obtained data were used for fitting the angular dependence of the resonance features using the EPR simulation tool "easyspin" with the embedded functions "resfield" and "pepper".[13] The simulation yielded the relative orientations of the individual **g** tensors with respect to an intrinsic simulation frame and that correlated with the spatial orientation of FeMo cofactor. The evaluation of spectra and assignment of relative orientations is detailed in the Supporting Information. The combination of two data sets (Figure 2 and Figure 3) resulted in an unambiguous assignment of the **g** tensor orientation with respect to the structure (Figures S1 and S4).

The $g_z=4.31$ component deviates by only 4.5° from the threefold axis of FeMo cofactor. This is within experimental error, due to the positional freedom of the crystal capillary in the EPR tube. Also, the $g_y=3.65$ component is only 16.5° out of the Fe1-C-S5 plane of the cofactor. As the magnetic tensor orientation is primarily determined by the atomic and electronic structure of FeMo cofactor, it was obvious that the observed, rhombic powder spectrum cannot fully reflect

the pseudo-D_3 symmetry of the cluster. Isolated FeMo cofactor retains its $S = 3/2$ spin state with large rhombicity in the absence of any protein ligand,[14] while an isolated [8Fe:9S:C] precursor that does not yet contain molybdenum is a far simpler $S = 1/2$ system.[15] It can thus be assumed that the heterometal plays a major role in establishing the high rhombicity of the $S = 3/2$ system, and that part of the asymmetry is attributed to the direct coordination by homocitrate and H442. However, the additional influence of the protein environment and the surrounding electrostatic potential field becomes apparent when comparing this data with that of holo-MoFe protein.[14] Mo contributes to orienting the g_z axis along the intrinsic threefold rotation axis of the cluster, but the surrounding amino acids will fine-tune in particular g_x and g_y. The g_y–g_z plane is near the cluster edge formed by atoms Fe1-Fe3-S5-Fe7-Mo (Figure 4) and introduces an asymmetry that cannot be deduced from the cluster structure alone.

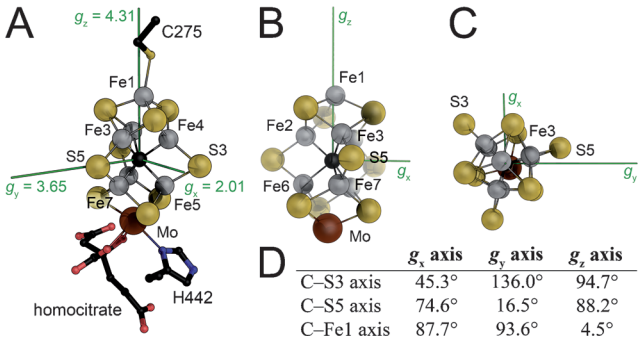

	g_x axis	g_y axis	g_z axis
C–S3 axis	45.3°	136.0°	94.7°
C–S5 axis	74.6°	16.5°	88.2°
C–Fe1 axis	87.7°	93.6°	4.5°

Figure 4. Orientation of the **g** tensor with respect to FeMo cofactor. A) Overall view including the immediate ligands to FeMoco. The g_z component deviates from the threefold axis of the cluster by only 4.5°. B) View along g_x. C) Top view of the cluster along g_z. The g_y axis deviates by 16.5° from the Fe1-Fe3-S5-Fe7-Mo edge of the cluster. D) Summary of the angles formed by the principal axes of the **g** tensor and intrinsic main axes of FeMo cofactor.

FeMo cofactor resides in a binding pocket that is predominantly lined by hydrophobic residues, with the exception of a small hydrophilic pocket above Fe3 which holds four water molecules in the structure of MoFe protein recorded at a resolution of 1.0 Å.[4b] Only a very limited set of conserved, putative electron donor ligands is present, namely α-Arg96, α-His195, α-Arg359, and α-His442 (Figure 5). The positively charged guanidine groups of the two arginine residues are located on either side of the Fe1-Fe3-S5-Fe7-Mo cluster edge, creating a local electrostatic potential environment that will reflect in the electronic structure of FeMo cofactor. The only amino acid side chains to directly ligate the cofactor are α-C275 and α-H442, supplemented by the organic (*R*)-homocitrate moiety (Figure 1 A). The high symmetry of FeMo cofactor precludes an unambiguous assignment of a substrate-binding site at its surface, and substrate binding has not been directly observed in wild-type MoFe protein. Studies on an α-V70 variant of the protein have pointed towards substrate and inhibitor binding to Fe6 in this mutant. The preference for Fe6 was supported by ^{13}CO

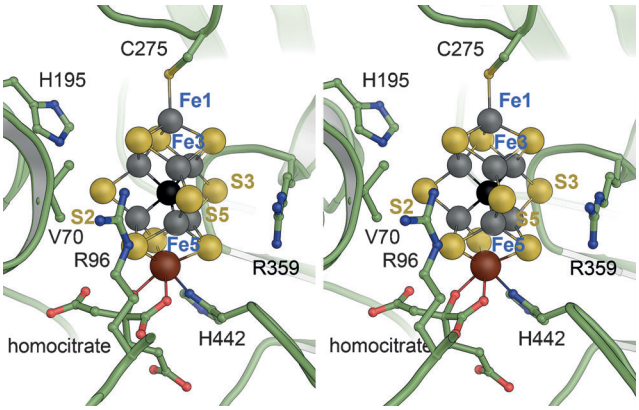

Figure 5. Putative electron-donor ligands surrounding the FeMo cofactor in the MoFe protein of nitrogenase. Direct coordination of the cluster is provided by only residues C275 and H442, but the conserved R96, H195, and R359 provide an anisotropic electrostatic environment that is likely to influence the **g** tensor orientation. Notably, the g_y axis is positioned along the Fe1-Fe3-Fe7-Mo cluster edge that is surrounded by the positively charged guanidino groups of R96 and R359. The figure is based on PDB entry 3U7Q.

incubation and the detection of its nuclear spin coupling to the electron spin of the cluster in ENDOR experiments,[16] but this analysis is necessarily strongly dependent on the available electronic model. In the present analysis, Fe6, located on the side facing residue α-H195, is close to the g_x axis of the tensor.

Since there is currently no satisfactory theoretical description of the electronic structure of FeMo cofactor, further experimental data is needed to serve as basis for refined computational approaches. The combination of X-ray diffraction and single-crystal EPR data of dithionite-reduced MoFe protein from *A. vinelandii* revealed, for the first time, the spatial orientation of the **g** tensor in the $S = 3/2$ FeMoco^N state with respect to its structure. This information can guide future DFT calculations to improve the quality of current electronic models. A refined electronic structure will fine-tune the description of the electron distribution within the cluster, including the resulting coupling behavior. It will also yield information about possible electron-transfer sites, all of which will be essential for a detailed understanding of substrate binding and activation.

Experimental Section

Cell growth and protein purification: *Azotobacter vinelandii* (Lipman 1903) was grown on Burke's medium in 500 mL flasks. The preculture medium was complemented with 10 mM NH_4Cl as the sole fixed-nitrogen source. Main cultures were complemented with 1.3 mM NH_4Cl leading to a de-repression of nitrogenase gene expression after ammonium depletion. Cells were harvested by centrifugation at an optical density (OD_{600nm}) of 3.0. The cell paste was washed with a 50 mM Tris/HCl buffer at pH 7.4. All subsequent steps were performed as described previously.[2]

Protein crystallization: All crystallization steps were carried out under anoxic conditions (95 % N_2/5 % H_2, < 5 ppm O_2). A 12 μL aliquot of protein solution (65 mg mL^{-1}) was mixed with the same volume of reservoir solution containing 0.7 M NaCl, 17.0 vol % PEG 4000, 3 vol % MPD, 0.2 M imidazole/malate buffer at pH 8.0, 0.55 mM

spermine, and 0.1 mM Zwittergent 3–14 (Hampton Research). All crystallographic steps were performed at 291 K using the sitting-drop vapor-diffusion method.[4b]

X-ray crystallography: Crystals were mounted in thin-walled (10 μm) quartz capillaries that were marked to indicate the initial position for X-ray and EPR data collection. Diffraction experiments were carried out on a MicroMax 007HF generator with a Saturn 944 + CCD detector (Rigaku) at 100 K. Data were treated as described previously.[4b]

EPR spectroscopy and data analysis: After X-ray data collection, the capillaries were transferred to X-band EPR tubes that were then filled with buffer containing 50 mM Tris/HCl at pH 7.4, 200 mM NaCl, and 5 mM $Na_2S_2O_4$. Data were recorded on a Bruker Elexsys E500 X-band spectrometer equipped with an Oxford Instruments helium cryostat at 7 K, microwave frequency 9.340 GHz; microwave power 50 mW, field modulation 100 kHz, modulation amplitude 8 G, time constant 328 ms, scan rate 179 G min^{-1}.

Received: April 10, 2013
Revised: June 11, 2013
Published online: August 8, 2013

Keywords: biological nitrogen fixation · EPR spectroscopy · FeMo cofactor · **g** tensor · magnetic properties

[1] a) J. B. Howard, D. C. Rees, *Chem. Rev.* **1996**, *96*, 2965 – 2982; b) D. C. Rees, F. A. Tezcan, C. A. Haynes, M. Y. Walton, S. Andrade, O. Einsle, J. B. Howard, *Philos. Trans. R. Soc. London Ser. A* **2005**, *363*, 971 – 984.

[2] O. Einsle, F. A. Tezcan, S. L. A. Andrade, B. Schmid, M. Yoshida, J. B. Howard, D. C. Rees, *Science* **2002**, *297*, 1696 – 1700.

[3] L. C. Seefeldt, B. M. Hoffman, D. R. Dean, *Annu. Rev. Biochem.* **2009**, *78*, 701 – 722.

[4] a) K. M. Lancaster, M. Roemelt, P. Ettenhuber, Y. L. Hu, M. W. Ribbe, F. Neese, U. Bergmann, S. DeBeer, *Science* **2011**, *334*, 974 – 977; b) T. Spatzal, M. Aksoyoglu, L. M. Zhang, S. L. A. Andrade, E. Schleicher, S. Weber, D. C. Rees, O. Einsle, *Science* **2011**, *334*, 940 – 940.

[5] a) J. M. Chan, J. Christiansen, D. R. Dean, L. C. Seefeldt, *Biochemistry* **1999**, *38*, 5779 – 5785; b) J. Rawlings, V. K. Shah, J. R. Chisnell, W. J. Brill, R. Zimmermann, E. Münck, W. H. Orme-Johnson, *J. Biol. Chem.* **1978**, *253*, 1001 – 1004; c) V. K. Shah, W. J. Brill, *Proc. Natl. Acad. Sci. USA* **1981**, *78*, 3438 – 3440.

[6] a) H. C. Angove, S. J. Yoo, E. Munck, B. K. Burgess, *J. Biol. Chem.* **1998**, *273*, 26330 – 26337; b) B. H. Huynh, E. Münck, W. H. Orme-Johnson, *Biochim. Biophys. Acta Protein Struct.* **1979**, *576*, 192 – 203; c) M. K. Johnson, A. J. Thomson, A. E. Robinson, B. E. Smith, *Biochim. Biophys. Acta Protein Struct.* **1981**, *671*, 61 – 70; d) S. J. Yoo, H. C. Angove, V. Papaefthymiou, B. K. Burgess, E. Munck, *J. Am. Chem. Soc.* **2000**, *122*, 4926 – 4936.

[7] a) B. H. Huynh, M. T. Henzl, J. A. Christner, R. Zimmermann, W. H. Orme-Johnson, E. Münck, *Biochim. Biophys. Acta Protein Struct.* **1980**, *623*, 124 – 138; b) W. E. Newton, S. F. Gheller, B. J. Feldman, W. R. Dunham, F. A. Schultz, *J. Biol. Chem.* **1989**, *264*, 1924 – 1927.

[8] a) H. B. I. Liu, A. Filipponi, N. Gavini, B. K. Burgess, B. Hedman, A. Dicicco, C. R. Natoli, K. O. Hodgson, *J. Am. Chem. Soc.* **1994**, *116*, 2418 – 2423; b) A. J. Pierik, H. Wassink, H. Haaker, W. R. Hagen, *Eur. J. Biochem.* **1993**, *212*, 51 – 61; c) V. Vrajmasu, E. Münck, E. L. Bominaar, *Inorg. Chem.* **2003**, *42*, 5974 – 5988.

[9] a) T. Lovell, T. Q. Liu, D. A. Case, L. Noodleman, *J. Am. Chem. Soc.* **2003**, *125*, 8377 – 8383; b) H. I. Lee, B. J. Hales, B. M. Hoffman, *J. Am. Chem. Soc.* **1997**, *119*, 11395 – 11400.

[10] S. J. Yoo, H. C. Angove, B. K. Burgess, M. P. Hendrich, E. Munck, *J. Am. Chem. Soc.* **1999**, *121*, 2534 – 2545.

[11] a) T. Lovell, J. Li, T. Q. Liu, D. A. Case, L. Noodleman, *J. Am. Chem. Soc.* **2001**, *123*, 12392 – 12410; b) L. Noodleman, C. Y. Peng, D. A. Case, J. M. Mouesca, *Coord. Chem. Rev.* **1995**, *144*, 199 – 244; c) L. Noodleman, *J. Chem. Phys.* **1981**, *74*, 5737 – 5743; d) J. M. Mouesca, L. Noodleman, D. A. Case, B. Lamotte, *Inorg. Chem.* **1995**, *34*, 4347 – 4359; e) J. M. Mouesca, L. Noodleman, D. A. Case, *Inorg. Chem.* **1994**, *33*, 4819 – 4830.

[12] R. J. Gurbiel, J. T. Bolin, A. E. Ronco, L. Mortenson, B. M. Hoffman, *J. Magn. Reson.* **1991**, *91*, 227 – 240.

[13] S. Stoll, A. Schweiger, *J. Magn. Reson.* **2006**, *178*, 42 – 55.

[14] A. W. Fay, M. A. Blank, C. C. Lee, Y. L. Hu, K. O. Hodgson, B. Hedman, M. W. Ribbe, *J. Am. Chem. Soc.* **2010**, *132*, 12612 – 12618.

[15] A. W. Fay, M. A. Blank, C. C. Lee, Y. L. Hu, K. O. Hodgson, B. Hedman, M. W. Ribbe, *Angew. Chem.* **2011**, *123*, 7933 – 7936; *Angew. Chem. Int. Ed.* **2011**, *50*, 7787 – 7790.

[16] H. I. Lee, L. M. Cameron, B. J. Hales, B. M. Hoffman, *J. Am. Chem. Soc.* **1997**, *119*, 10121 – 10126.

